AD-A167 272 STRUCTURAL INSTABILITIES IMPURITIES AND DEFECTS IN ELECTRONIC MATERIALS(U) UTAH UNIV SALT LAKE CITY DEPT OF PHYSICS P C TAYLOR 14 AUG 85 N00014-83-K-0535 1/1

UNCLASSIFIED F/G 20/12 NL

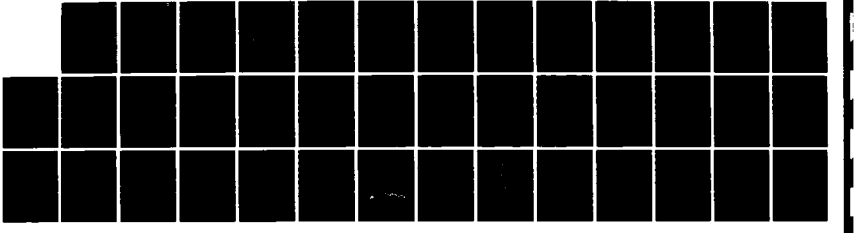

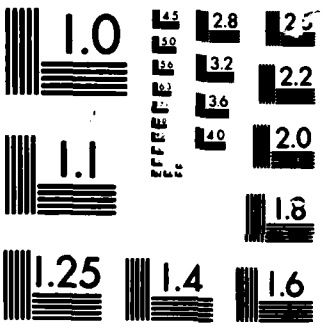

MICROCOPY CHART

STRUCTURAL INSTABILITIES, IMPURITIES AND DEFECTS IN ELECTRONIC MATERIALS

Final Report for Contract Period

15 August 1983 - 14 August 1985

Contract No. N00014-83K-0535

Principal Investigator: P.C. Taylor

Associate Principal Investigator: William D. Ohlsen

Department of Physics
University of Utah
Salt Lake City, UT 84112

CUMULATIVE LIST OF PUBLICATIONS FOR

Contract No. N00014-83-K-0535

83-K-0535-1: "Photoluminescence Study of Confined Electron Hole Plasma in $Ga_xIn_{1-x}As$ Heterostructures," M. Gal, J.M. Viner, P.C. Taylor, C.P. Kuo, R.M. Cohen and G.B. Stringfellow, J. Appl. Phys. 58, 948 (1985).

83-K-0535-2: "Magnetic Effects in Non-Crystalline Semiconductors," P.C. Taylor in Amorphous Semiconductors, M. Pollak, ed. (CRC Press, NY, 1985), in press.

83-K-0535-3: "Nuclear Quadrupole Resonance in the Chalcogenide and Pnictide Amorphous Semiconductors," P.C. Taylor in Physics and Chemistry of Disordered Systems, D. Adler, H. Fritzsche, and S.R. Ovshinsky, eds. (Plenum Press, NY, 1985), p. 517.

83-K-0535-4: "Optical Properties of Non-Crystalline Semiconductors," P.C. Taylor in Amorphous Semiconductors, M. Pollak, ed. (CRC Press, NY, 1985), in press.

83-K-0535-5: "Defects in Tetrahedrally Coordinated Amorphous Semiconductors," P.C. Taylor in Materials Issues in Applications of Amorphous Silicon Technology, D. Adler, A. Madan, and M.J. Thompson, eds. (Materials Research Society, Pittsburgh, 1985), p. 61.

83-K-0505-6: "Doping Superlattices in Organometallic VPE InP," J.S. Yuan, M. Gal, P.C. Taylor and G.B. Stringfellow, Appl. Phys. Lett. 47, 405 (1985).

83-K-0535-7: "Modulated Reflectance Spectroscopy of InP Doping-Superlattices," M. Gal, J.S. Yuan, J.M. Viner, P.C. Taylor and G.B. Stringfellow, Phys. Rev. Lett. (1985), submitted.

TABLE OF CONTENTS

I. INTRODUCTION

The research supported under the present contract has been directed toward an understanding of some basic optical properties in materials of potential importance to the development of electronic devices. One important class of materials studied has been thin films of III-V semiconductors which are grown using organometallic transport gases. These materials have been investigated using both individual layers and multiple-layer structures. In the layer structures, some effects due to the quantum confinement of electrons have been studied.

A second class of materials studied has been amorphous semiconductors. In this class of solids we have investigated diffusion of impurities in oxide glasses and amorphous silicon films. Research has also been performed on the effects of light on the optical and structural properties of thin layers of chalcogenide glasses.

II. OPTICAL PROPERTIES OF III-V SEMICONDUCTORS GROWN BY OMCVD

During the course of the present contract we have initiated a collaborative effort with the materials preparation and characterization group headed by Professor Gerald Stringfellow in the Materials Science and Engineering Department at the University of Utah. Professor Stringfellow and his group grow III-V semiconductors by organometallic vapor phase epitaxy (OMVPE). This group has been growing layered structures in various ternary and quaternary systems, and recently has developed the capability of producing superlattices. Together we have shown the use of a novel structure to study a confined electron-hole plasma in semiconducting heterostructures,[1] reported the first doping superlattices ever grown by OMVPE,[2] and demonstrated the great potential of the photoreflectance

technique for probing details of the quantum size effects in these structures.[3]

A. Electron-Hole Plasma in Thin Layers of $Ga_yIn_{1-y}As$

The electron-hole plasma was studied in a novel heterostructure confined in a 500 Å $Ga_yIn_{1-y}As$ layer sandwiched between an InP substrate and a wider gap $Ga_xIn_{1-x}As$ layer. This structure is shown in Fig. 1. The identification of a specific photoluminescence (PL) process as due to an electron-hole plasma is the result of analyses of the intensity and the temperature dependences of the PL, the effect of a magnetic field on the heterostructure and polarization properties of the emitted light.

The $Ga_xIn_{1-x}As$ layers were grown by organometallic vapor-phase epitaxy (OMVPE). Because the carriers are confined to a thin layer, one can observe PL from an EHP at much lower pumping intensities than is commonly the case for three-dimensional samples. In addition, the observation of efficient PL from an EHP implies that competing nonradiative processes at the interfaces are unimportant. This observation thus provides a graphic demonstration of the high interfacial quality which can be achieved by the OMVPE growth technique.

In highly excited indirect-gap semiconductors, such as Ge and Si, a luminescence line, which appears at slightly lower energies than that of the free exciton, has been identified as an emission from an electron-hole liquid.[4] This situation is in contrast to direct-gap materials, where the very short carrier lifetime usually prevents phase separation between the free exciton gas and the electron-hole liquid. At high intensities the excitons dissociate into an EHP, composed of free electrons and holes.

In a bulk semiconductor, substantial EHP density only occurs at very high excitation intensities due to the short lifetime and the rapid

diffusion of the carriers out of the photoexcited volume. Typical excitation intensities in a bulk semiconductor can reach the kW or even the MW range. By confining the carriers in a potential well, we have observed EHP luminescence at several orders of magnitude lower pump intensities and thus we were able to use cw excitation instead of the usual pulsed excitation. As a result, our measured spectra were independent of the time evolution of the exciton-EHP system that often complicates the description of this phenomenon.[5]

For an unintentionally doped n-type sample at T = 2K, Fig. 2(b) shows a typical PL spectrum excited at the lowest power densities (P_1 = 20 mW/cm^2). At these power levels only the emission from the top layer is observed. The spectrum of Fig. 2(b) shows an exciton line at hv = 0.82 eV, and an impurity-related line lower in energy by about 20 meV. The excitonic nature of the dominant high-energy line is supported by the observed excitation and temperature dependences.[2]

The PL spectra change dramatically upon increasing the pump intensity. Figure 2(a) shows the result of changing the excitation intensity by a factor of 100. A new emission band appears at lower energies, which at the highest excitation intensities dominates the emission. The dependence of this new band on excitation power can be seen in Fig. 3, where the logarithm of the emission intensity is plotted as a function of wavelength for different pumping intensities. As can be seen from this figure, the peak of the emission moves to higher energy (longer wavelength) with increasing excitation intensity, while at the same time, the low-energy "tail" of this emission changes very little with excitation intensity.

The temperature dependence of this new band was studied between 2 and 80K. The integrated intensity varied only slightly with temperature over

this range, with some samples showing an increase in the emission intensity as the temperature was raised.

In light of these observations, we have suggested that this new emission band is due to an EHP confined between the two higher band-gap materials.[1] This identification implies that the interfaces between the InP substrate and the thin layer, and between the thin layer and the thicker $Ga_{0.47}In_{0.53}As$ top layer are of high quality (i.e., with a low interface recombination velocity). If this were not the case, then one would expect competing surface-related processes to dominate the recombination. For a semi-insulating InP substrate, and undoped, slightly n-type GaInAs layers, the heterostructure would look schematically like that shown in Fig. 1(b). (The effects of band-bending have been neglected in the figure for these undoped layers.) Since the absorption coefficient is approximately 10^5 cm^{-1} at the energy of excitation ($h\nu = 2.41$ eV), the nominal penetration depth of the laser light is approximately $d \approx 0.1$ μm. Thus, at low pumping intensities only the top layer is excited, and this excitation condition will give rise to the exciton and impurity-related emission bands characteristic of the top layer. At higher pumping intensities, an increasing number of photogenerated carriers diffuses from the top layer and gets collected in the potential well formed by the conduction band discontinuity. Since the width of the potential well is only ~ 500 Å, the carrier density becomes substantial even at relatively low pumping power levels.

In order to evaluate the plasma density and plasma temperature of the confined EHP, we have fitted the measured luminescence band to an expression which describes radiative recombination from an EHP in the absence of

momentum conservation.[6] The fits as shown in Fig. 4 are quite good except at low energies. Details are available in ref. 1.

It is interesting to note that the plasma temperature used in fitting the curves of Fig. 4 agrees closely with the bath temperature for all samples and temperatures studied. In most highly excited semiconductors, when the excitation energy is well above the band gap, the electronic temperature is found to increase above the bath temperature.[5] This increase is due to the heating of the plasma (either directly or indirectly) by the hot electrons (and holes) that are created by the exciting photon. In our case however, the energy difference between the laser photon and the band gap of GaInAs is dissipated in the top layer and subsequently by the He, and thus the carriers captured into the potential well are "cool." The excess energy of the electrons and holes forming the EHP is only of the order of 50 meV, which is not enough to heat up the electronic system substantially.

Additional evidence that the observed emission is indeed from the potential well, and not from an as yet unidentified emission of the top layer, is provided by externally hindering the drift of the carriers toward the lower gap layer. An effective way of reducing the number of carriers arriving at the potential well can be achieved by applying a magnetic field parallel to the sample layer, i.e., normal to the diffusion path of the carriers. As a result, the diffusion length is reduced by the magnetic field.[7] In a magnetic field one expects the EHP luminescence to decrease and shift to lower energy, and the exciton luminescence of the top layer to increase.[7]

Our results, conducted in a magnetic field of 2.5 T parallel to the layer structure, confirm this expectation, as can be seen in Fig. 5. At

this value of the magnetic field, the EHP luminescence was decreased by approximately 40%, while the exciton luminescence was found to increase.

In summary, we have observed EHP emission from a 500 Å thick layer of $Ga_yIn_{1-y}As$ confined between InP and $Ga_{0.47}In_{0.53}As$ layers. Since the emission was observable even at low power levels ($\geq$ 300 mW/cm^2), we conclude that the collection efficiency of the potential well was substantial, and thus the heterojunction interface was of high quality. A line shape analysis of the EHP emission yields electronic temperatures which essentially coincide with the bath temperatures.

B. Doping Superlattices in InP

In collaboration with Professor Stringfellow we have investigated the first doping superlattices grown by organometallic vapor phase epitaxy (OMVPE). The superlattices were grown in InP with layer thicknesses as small as 200 Å. The 4K PL peak energy was found to be considerably less than the band gap of homogeneous InP and to depend on excitation intensity. The luminescence was found to decay in distinct stages, each stage being approximately exponential, with a range of time constants from 6×10^{-8} to 7×10^{-4} s at 4K, as expected for transitions which are indirect in real space between different quantum levels.

The PL for a single superlattice with n- and p-layer thicknesses of 200 Å and doping levels of 1×10^{18} and 2×10^{18} cm^{-3}, respectively, is described as an example. The PL was excited using the 514 nm line of an Ar^+ laser at powers ranging from 0.6 to 600 mW. The laser was focused to a spot ~ 100 μm in diameter, giving excitation intensities ranging from 6 to 6000 W/cm^2.

The PL spectra are shown at various excitation intensities in Fig. 6. In each case the spectrum consists of a single peak. The highest energy

peak, measured at an excitation intensity of 600 mW, is located at 888 nm or 1.395 eV. This is somewhat below the free-exciton emission in InP, which at 4K is 1.418 eV. The peak shifts to lower energy and broadens as the excitation intensity decreases. At 0.6 mW, the peak is shifted to 1.326 eV, 69 meV lower than at the highest excitation intensity. The peak position is plotted versus excitation intensity in Fig. 7. The slope of the line is similar to that reported by Yamauchi et al.[8] for 77K PL measurements for layers doped to 5×10^{17} cm^{-3} and for layer thicknesses of 300-4000 Å. The data are also similar to those obtained for GaAs doping superlattices,[9] i.e., approximately 25 meV per decade of pumping intensity. The peak positions reported here occur at lower energies than those reported by Yamauchi et al.[8] for similar layer thicknesses, presumably due to the higher doping levels of our superlattices.

The decay of the PL signal measured at 4K is shown in Fig. 8. The decay clearly has a rapid exponential stage with a time constant of less than 6×10^{-8} s followed by additional exponential stages with time constants of 4.5×10^{-6} and 7×10^{-4} s. Such extremely long decay times are expected for recombination of electrons and holes which are spatially separated.[10] The discontinuities in the slope of the PL versus time may be due to changes in the carrier concentration as the different subbands become depopulated, as predicted theoretically.[11]

In summary, the first doping superlattices obtained by OMVPE exhibit a single PL peak at 4K which shifts from 1.326 eV at a laser excitation intensity of 0.6 mW to 1.395 eV at 600 mW. The free-exciton emission in InP at 4K is 1.418 eV. The PL decay consists of a series of three exponential steps with time constants ranging from 6×10^{-8} to 7×10^{-4} s.

C. Photoreflectance in InP Doping Superlattices

Electroreflectance (ER) and photoreflectance (PR) are valuable and venerable techniques for understanding interband transitions in bulk semiconductors. However, detailed lineshape analyses are difficult for bulk semiconductors because the modulation of the reflection is caused by surface fields which are often hard to characterize.[1-3] Recently there have been several applications of the ER[4,5] and PR[6] techniques to semiconductor superlattices, or quantum well structures, mainly in the GaAs-$Ga_{1-x}Al_xAs$ system. Here again, although a wealth of information can be obtained concerning characteristic energies for the various interband transitions, detailed lineshape analyses are complicated by a variety of factors including the nature of the electric fields and the presence of overlapping transitions of different types.

The photoreflectance (PR) technique is very similar to the well known electro-modulation technique, which produces derivative-like features in the reflectivity spectra near the vicinity of the interband transitions. PR, which can easily be performed at room temperature, can be considered as a contactless form of electro-modulation in which the modulation is produced by the photoinjected carriers.

We have demonstrated the first application of the PR technique to doping superlattices (so-called nipi structures). This class of superlattices has a tunable optical band-gap, which depends on the free carrier concentration, and extremely long minority carrier lifetimes due to the spatial separation between electrons and holes in the n and p layers. In addition to these unique features, the nipi superlattices also exhibit quantum size effects similar to those observed in quantum wells.

Because optical modulation in the doping superlattices affects the real-space modulation of the band gap and the population of the subband levels in a very predictable fashion,[10,12] a detailed and semi-quantitative understanding can be obtained. The optical modulation with band gap light produces electrons and holes which modulate the electric fields generated in the superlattice by the spatial distribution of the dopants. This effect in turn modulates the position of the electronic subbands in the conduction band and contributes to a modulation of the reflectivity in the vicinity of these subband levels.

The PR spectra also allow us to identify the allowed transitions between the valence band and quantized subbands of the conduction band. The results presented here for InP doping superlattices made by the OMVPE process illustrate the potential of the PR technique for probing quantum confinement in these layer structures.

Figure 9 shows the PR spectrum of an InP doping superlattice at 80K. The n- and p-doping levels are 1×10^{18} cm^{-3} and 2×10^{18} cm^{-3}, respectively. The thicknesses of the n- and p-layers are $d_n = d_p = 20$ nm. The spectrum shown in Fig. 9 was observed using 1.2 W cm^{-2} at 2.41 eV (5145 Å) as the modulation source. The intensity in $\Delta R/R$ at low energies ($\leq$ 1.35 eV) is due to photoluminescence (PL) from the doping-super-lattice structure as described in the previous section. The weak structure near and below ~ 1.41 eV is due to the well known E_o transition in the bulk InP substrate. This structure, which is also apparent in Fig. 10, is similar to the ER lineshapes observed in bulk InP. Note from Fig. 10 that at room temperature the PL is unobservable and the PR lines shift to lower energy. The measured shift is similar to that observed in the ER spectra of bulk InP and is due to the temperature dependence of the band gap.

Above the bulk band gap of InP (E_g^o), several PR lines are observed in Fig. 9. Unlike the case of PR in bulk semiconductors, these lines are strongly dependent on the modulated light intensity as shown in Fig. 11. At lower intensities the PR lines become narrower and additional features appear (Fig. 11). These features, which we will show are due to transitions between the valence band (and the split-off valence band) and the quantized subbands of the conduction band, can be calculated using known expressions for doping superlattices.[10] For the sample used in Figs. 9-11 we calculate that there will be at most five quantized levels in the conduction band with the existence of the fifth level problematical because of uncertainties in the values of the experimental parameters. The situation is shown schematically in the inset to Fig. 11. The quantity E^{Δ} is the energy difference between the valence band the split-off valence band. Transitions from the valence band and split-off valence band to the subband levels of the conduction band are denoted by the indices n and n^{Δ}, respectively. (We ignore the quantized subbands in the valence band because their splittings in InP are an order of magnitude smaller than those of the conduction band.) The transition energies are given by[11]

$$E^n = E_g^o + E_c^n \tag{1}$$

where

$$E_c^n = h\left[\frac{4\pi e^2 N_D}{\kappa_o m_c^*}\right]^{1/2}\left(n + \frac{1}{2}\right) \qquad n = 0,1,2,\cdots \tag{2}$$

and where we have ignored the contribution due to subbands in the valence band. In Eq. (1) E_g^o is the band gap energy of bulk InP and E_c^n is the energy

of the n^{th} subband level with respect to the conduction band minimum. In Eq. (2) N_D is the donor concentration, κ_o the low frequency dielectric constant and m_c^* the conduction band effective mass.

Equation (2) predicts a shift in the subband levels with doping which depends on $N_D^{\frac{1}{2}}$. As shown in Fig. 12, this shift is observed in the PR spectra. Superimposed in Fig. 12 are the n = 1 transitions at low modulation intensity for two samples with $N_D \sim 1 \times 10^{18}$ cm^{-3}, respectively. The observed shift of ~ 15 meV is consistent with the predictions of Eq. (2).

For the sample whose results are displayed in Figs. 9-11 the appropriate parameters for Eqs. (1) and (2) are $E^{\Delta} = 0.11$ eV, $2E_c^o = 46$ meV and $E_g^o = 1.41$ eV at 80K (1.31 eV at 300K). The positions of the various transitions at 80K are shown in Fig. 11.

It is not immediately apparent that the observed spectral features in Fig. 11 are uniquely explained by the transitions as listed. For this reason we have calculated the expected lineshape using a simple model of Lorentzian oscillators which was originally developed for ER of excitons.[13] If the transitions to the n^{th} subband are characterized by an oscillator strength f_n and occur at energy $\hbar\bar{\omega}_n$, then the normalized changes in the reflectivity due to a modulation of the n^{th} subband energy can be expressed as[13]

$$\frac{\Delta R}{R} \propto \sum_n |f_n|^2 \Gamma_n^{-3} \left[\frac{w^2(n) - 1}{(w^2(n) + 1)^2} \right] \tag{3}$$

where

$$w(n) = \left(\frac{2}{\Gamma_n} \right) \left(\omega - \bar{\omega}_n \right) \tag{4}$$

and where Γ_n is a broadening parameter (linewidth). We ignore the contribution to the PR lineshape due to any modulation of the broadening parameter because the subband energies are known to be a strong function of the light intensity,[14] and this effect should dominate the lineshapes in the doping superlattices. It is interesting to note that the lineshapes associated with each transition are very similar to those observed in ER and PR of bulk semiconductors in the high field regime.[15]

The oscillator strengths f_n are not easily calculable but one general comment can be made. For the perfectly symmetric situation one would expect only even harmonic oscillator functions to contribute, which would result in the observation of every other subband. However, we observe contributions to $\frac{\Delta R}{R}$ from all subband levels. We believe this situation results from an assymmetry in the doping profile which is inherent in the growth procedure.

Since little is known concerning the excited levels in the valence band, we have fit the spectrum in Fig. 11 with appropriate values for the parameters.[3] One should not place too much emphasis on the intensities of the various transitions for our somewhat arbitrary choice of transition probabilities. On the other hand, the calculated inflection points, which correspond closely to those observed experimentally, are essentially independent of the transition probabilities.

At higher modulation intensities the energy separations between subbands decrease logarithmically.[16] Figure 9 shows the lineshape calculated with essentially the same parameters used in the low intensity curve of Fig. 11 but with $2E_c^o$ = 18 meV as the model calculations indicate.[16] The experimental trace is accurately reproduced in the model calculation.

In summary, we have demonstrated the great potential of the PR technique for studying quantum size effects in doping superlattices. The

observed PR lineshapes are well explained by photomodulation of the subbands in the conduction band. More extensive studies may yield detailed information concerning electronic wave functions both for excited states near the valence band maximum (in real space) and for the quantized subbands of the conduction band.

III. METASTABILITIES IN AMORPHOUS SOLIDS

By their very nature, amorphous solids are metastable, and such meta-stabilities affect the structural, vibrational and electronic properties. In practical applications the metastable nature of amorphous solids is often a liability. For example, hydrogen diffusion into optical fibers produces an absorption which greatly degrades the performance. The efficiency of hydrogenated amorphous silicon (a-Si:H) solar cells degrades when the cells are irradiated with light because of a change in the electronically active defects in these amorphous films. The structure of glassy chalcogenide films can sometimes be altered with the application of light of energy equal to, or greater than, that of the band gap. Some of the research efforts of the present contract have been directed toward an understanding of these meta-stable changes.

A. Diffusion of Molecular Hydrogen in Amorphous Solids

Diffusion of molecular hydrogen (H_2) in amorphous solids has become of considerable practical importance since the realization that H_2 diffusion onto quartz fibers is a potential failure mode for undersea optical cables. During the contract we have demonstrated the utility of ^1H NMR for investigating the diffusion of molecular hydrogen (H_2) in several amorphous solids. Results have been obtained on a representative amorphous insulator (7059 glass) and on a representative amorphous semiconductor (hydrogenated

amorphous silicon or a-Si:H). In what follows we use the a-Si:H data as an example because they emphasize the utility of this technique in thin film geometries.

In most films of a-Si:H molecular hydrogen exists at levels on the order of 10^{-2} to 10^{-1} at.%. Most of the hydrogen, however, is bonded to silicon atoms. Typical films contain approximately 10 at.% of bonded hydrogen.

Some of the H_2 molecules in a-Si:H can be probed by examining the spin lattice relaxation rates T_1^{-1} of hydrogen bonded to the silicon network.[17] It has been established that a characteristic minimum in T_1 near 40K is due to the relaxation of the bonded hydrogen atoms via some of the H_2 molecules trapped in the films. A typical example of this T_1 minimum is shown in Fig. 13. It can be shown that the magnitude of the minimum value of T_1 is proportional to that concentration of H_2 molecules which is effective in relaxing the bonded hydrogen.

The data of Fig. 13 shows that there are fewer H_2 molecules effective in relaxing the bonded hydrogen in flakes of a-Si:H which have been removed from the substrate than in similar films which remain on the substrate. We have postulated that removal of the films from the substrate provides a strain relief mechanism which allows some of the trapped H_2 to diffuse out of the films. This speculation is supported by the fact that one can also achieve the same decrease in trapped H_2 concentration by allowing the films on the substrate to "age" for ten months (circles in Fig. 13).

After the films have aged, one can reinduce H_2 by immersing the sample in an atmosphere of H_2 or by heating the samples and creating H_2 from bonded hydrogen.[18] This "diffusion" process takes only about three weeks at room temperature with approximately one atmosphere pressure of H_2. Molecular

hydrogen can be reintroduced into the film by either of these two processes only up to the level observed in the virgin films. Futhermore, the reintroduced hydrogen is not stable and diffuses out at room temperature on a time scale of a few weeks. This process is much faster than the initial aging process.

Even in the best films of a-Si:H there are regions where there are no atoms. The dimensions of these voids are not well characterized , but their presence is well established. We have speculated[18,19,20] that the stress relief involved in the initial aging process results in a relaxation of the initial void structure such that future reinducing can proceed more rapidly but that the molecular hydrogen is no longer as strongly trapped. Because the reinducing process appears to saturate and because the temperature dependence doesn't yield parameters consistent with a simple diffusion process, a more complicated mechanism will be necessary to explain the aging effect in a-Si:H.

B. Photo-Induced Structural Changes in Amorphous Semiconductors

In the chalcogenide glasses the photodarkening (PD) process refers to a shift of the optical absorption edge to lower energies upon the application of light whose energy is near that of the band gap. All chalcogenide glasses appear to exhibit the PD process to varying degrees. The process has even been observed in some oxide glasses such glassy As_2O_3. However, the presence of a group VI element appears to be necessary to observe the PD effect since amorphous arsenic (a-As) and amorphous silicon (a-Si) do not exhibit photodarkening.

The role of specific defects in the photodarkening process has yet to be established because a microscopic description of this effect does not yet exist. Over the years several possibilities have been suggested including

"dangling" chalcogen atoms and under- and over-coordinated chalcogen atoms. In addition, evaporated or sputtered amorphous chalcogenide films often exhibit more gross photo-induced structural rearrangements, such as photo-polymerization, which do not occur in bulk glassy chalcogenides. In the present contract we have concentrated on the more subtle PD effect which occurs in bulk chalcogenide glasses.[21,22]

In well-annealed bulk chalcogenide glasses gross structural rearrangements, such as photopolymerization, do no occur, but there are more subtle changes in many optical and electrical properties which do occur under the influence of light. Most of these changes are reversible either by irradiation with light of energies less than that of the band gap or by annealing at temperatures below the glass transition temperature, T_g.

The PD effect appears to saturate after a given time. An example of this apparent saturation is shown in Fig. 14. The fact that this saturation is an apparent one, and not real, is illustrated for glassy As_2S_3 in Fig. 14. This figure shows the optical absorption coefficient in glassy As_2S_3 at 85K after several irradiation times. Curves 7 and 8 were taken after 173 and 292 min. irradiation, respectively, with 2.41 eV light, and they are essentially indistinguishable. The additional PD effect shown in curve 9 was obtained by irradiating the sample from the opposite side from that used in curves 1 through 8. This experiment clearly demonstrates that the saturation is in this case an apparent one which involves the collapse of the penetration depth of the exciting light as the absorption coefficient near the irradiated surface increases dramatically.

Recently we have been studying subtle changes in the As-S bonding which may occur in glassy As_2S_3 upon photodarkening. These subtle changes are being probed through the use of ^{75}As pulsed nuclear quadrupole resonance

(NQR) techniques. Although these are no gross bonding rearrangements such as the photopolymerization which occurs in films of As_2S_3, we hope to observe the subtle changes in the non-bonding valence band of this amorphous semiconductor.

We have also been investigating the microscopic nature of defects created during the PD process. The experimental technique which we employ in these experiments is electron spin resonance (ESR). Preliminary measurements have indicated that several ESR centers are created during the PD process, but for most of them, the kinetics of creation and annelaing do not match those of the PD effect. There appear to be one chalcogen-related center and perhaps one arsenic-related center which do correlate well with the kinetics of the PD effect. These experiments are continuing, and we hope in this fashion to obtain a microscopic picture for the PD effect in the near future.

IV. SUMMARY

During the course of the present contract a cooperative research effort has been established with Professor Gerald Stringfellow in the Department of Materials Science and Engineering at the University of Utah. This cooperative effort has resulted in several research achievements including (1) the observation of an electron-hole plasma in a confined (500 Å) layer of $Ga_yIn_{1-y}As$ sandwiched between two larger band gap layers, (2) the first observation of a doping superlattice in material grown by the OMVPE technique, and (3) the detailed characterization of these doping superlattices using photoreflectance techniques. The second result demomstrates that our research effort can play a leading role in the investigation of the optical properties of layer structures grown by OMVPE. The third result

clearly demonstrates that the electronic fields which exist in the doping superlattices can be very well characterized by the photoreflectance technique.

The contract has also resulted in research into the metastabilities present in amorphous solids. The important achievements in this area include (1) the use of ^{1}H NMR to study the diffusion of molecular hydrogen (H_2) in hydrogenated amorphous silicon and oxide glasses, (2) a preliminary study of photo-induced structural changes in chalcogenide glasses using optical, NQR and ESR techniques. An understanding of the diffusion of H_2 in amorphous solids may be important for ultimately controlling the degradation of optical fibers in an under-sea environment. An understanding of the photostructural processes in chalcogenide glasses may have significance in efforts to develop inorganic photoresists.

REFERENCES

1. M. Gal, J.M. Viner, P.C. Taylor, C.P. Kuo, R.M. Cohen and G.B. Stringfellow, J. Appl. Phys. 58, 948 (1985).

2. J.S. Yuan, M. Gal, P.C. Taylor and G.B. Stringfellow, Appl. Phys. Lett. 47, 405 (1985).

3. M. Gal, J.S. Yuan, J.M. Viner, P.C. Taylor and G.B. Stringfellow, Phys. Rev. Lett. (1986), submitted.

4. D.C. Reynolds and T.C. Collins, Excitons, Their Properties and Uses (Academic, New York, 1981).

5. O. Hildebrand, E.O. Goebel, K.M. Romanek, H. Weber and G. Mahler, Phys. Rev. B17, 4775 (1978).

6. T.K. Lo, Solid State Commun. 15, 1231 (1974).

7. B. Lax and J.G. Mavroides in Solid State Physics, Vol. 11, edited by F. Seitz and D. Turnbull (Academic Press, New York, 1960), p. 261.

8. Y. Yamauchi, K. Uwai and O Mikami, Jpn. J. Appl. Phys. 23, L785 (1984).

9. H. Jung, H. Kunzel, G.H. Döhler and K. Ploog, J. Appl. Phys. 54, 6965 (1983).

10. G.H. Döhler, J. Vac. Sci. Technol. B1, 278 (1983).

11. W. Rehm, P. Ruden, G.H. Döhler and K. Ploog, Phys. Rev. B28, 5937 (1983).

12. G.H. Döhler, Phys. Stat. Solidi b52, 79 (1972); 533 (1972).

13. M. Cardona, Modulation Spectroscopy, Solid State Physics, Suppl, 11, F. Seitz, D. Turnbull and H. Ehrenreich, eds. (Academic, New York, 1964), p. 110.

14. K. Ploog, Ann. Rev. Mater. Sci. 12, 123 (1982).

15. D.E. Aspnes and A. Frova, Phys. Rev. B2, 1037 (1970).

16. G.H. Döhler, H. Künzel, D. Olego, K. Ploog, P. Ruden and H.J. Stolz, Phys. Rev. Lett. 47, 864 (1981).

17. W.E. Carlos and P.C. Taylor, Phys. Rev. B25, 1435 (1982).

18. E.D. VanderHeiden, W.D. Ohlsen and P.C. Taylor, Bull. Am. Phys. Soc. 30, 354 (1985).

19. P.C. Taylor in Amorphous Semiconductors, M. Pollak, ed. (CRC Press, New York, 1986) in press.

20. P.C. Taylor in Materials Issues in Applications of Amorphous Silicon Technology, Vol. 49, D. Adler, M. Madan and M.J. Thompson, eds. (Materials Research Society, Pittsburgh, 1985), p. 61.

21. P.C. Taylor in Physics of Disordered Materials, D. Adler, H. Fritzsche, and S.R. OVshinsky eds. (Plenum, New York, 1985), p. 517.

22. P.C. Taylor in Amorphous Semiconductors, M. Pollak, ed. (CRC Press, New York, 1986) in press.

23. J.Z. Liu and P.C. Taylor, Proc. Int. Conf. on Amorph. and Liquid Semicond., A. Frova, ed. (North Holland, London, 1986), in press.

FIGURE CAPTIONS

Fig. 1. (a) Schematic structures of typical $Ga_xIn_{1-x}As$ heterostructures. (b) Schematic band diagrams for the structures of part a.

Fig. 2. Typical PL spectra under two different excitation intensities: (a) excitaion intensity I_o = 2 W/cm^2, (b) I_o = 20 mW/cm^2.

Fig. 3. Low-energy emission lineshape as a function of excitation intensity in $Ga_xIn_{1-x}As$ heterostructures.

Fig. 4. Luminescence spectra at constant excitation intensity for different temperatures. The circles represent the experimental points, while the solid curves are the calculated EHP lineshapes using parameters given in the figure. See ref. 1 for details.

Fig. 5. The effect of a magnetic field on the EHP emission intensity.

Fig. 6. Photoluminescence spectra measured at 4K with various excitation intensities for an InP doping superlattice with layer thicknesses of 200 Å and n- and p-doping levels of 1×10^{18} and 2×10^{18} cm^{-3}, respectively.

Fig. 7. Photoluminescence peak position vs. excitation intensity in an InP doping superlattice.

Fig. 8. Photoluminescence intensity vs time after removal of excitation.

Fig. 9. Low Temperature (80K) PR spectrum at high modulation intensity in an InP doping superlattice. E_g^o denotes the band gap of bulk InP. The lower trace is a calculated spectrum based on the model described in the text.

Fig. 10. Room temperature PR spectrum at high modulation intensity in an InP doping superlattice.

Fig. 11. Low temperature (80K) PR spectrum at low modulation intensity in an InP doping superlattice. E_g^o denotes the band gap of bulk InP. The indices n and n^Δ refer to transitions from, respectively, the valence band and the split-off valence band to the subband levels in the conduction band. The lower trace is a calculated spectrum based on the model described in the text.

Fig. 12. Comparison of low energy portions of room temperature PR spectra at ~ 1 mW cm^{-2} modulation intensity for two doping superlattices of different doping concentrations. (a) $N_D \sim 1 \times 10^{18}$ cm^{-3}, (b) $N_D \sim 2 \times 10^{18}$ cm^{-3}.

Fig. 13. ^1H spin lattice relaxation time in a-Si:H as a function of temperature. The solid line represents data on flakes which have been removed from the substrate. Triangles indicate data taken on films on quartz substrates within two weeks of deposition. Circles denote data taken on the same films after ten months. The magnitude of the minimum value of T_1 (near 40K) is inversely proportional to the number of H_2 molecules contributing to the relaxation process.

Fig. 14. Optical absorption coefficient as a function of energy for different irradiation times in glassy As_2S_3 at 85K. The irradiation energy was 2.41 eV at an intensity of 150 mW/cm^2. Curves 1 through 8 represent irradiation times of 0;60;150;400;1,000;4,600;10,400 and 17,500 sec., respectively. Curve 9 (dashed) represents an additional irradiation of 13,200 sec. from the opposite side of the sample. See text for details. After ref. 23.

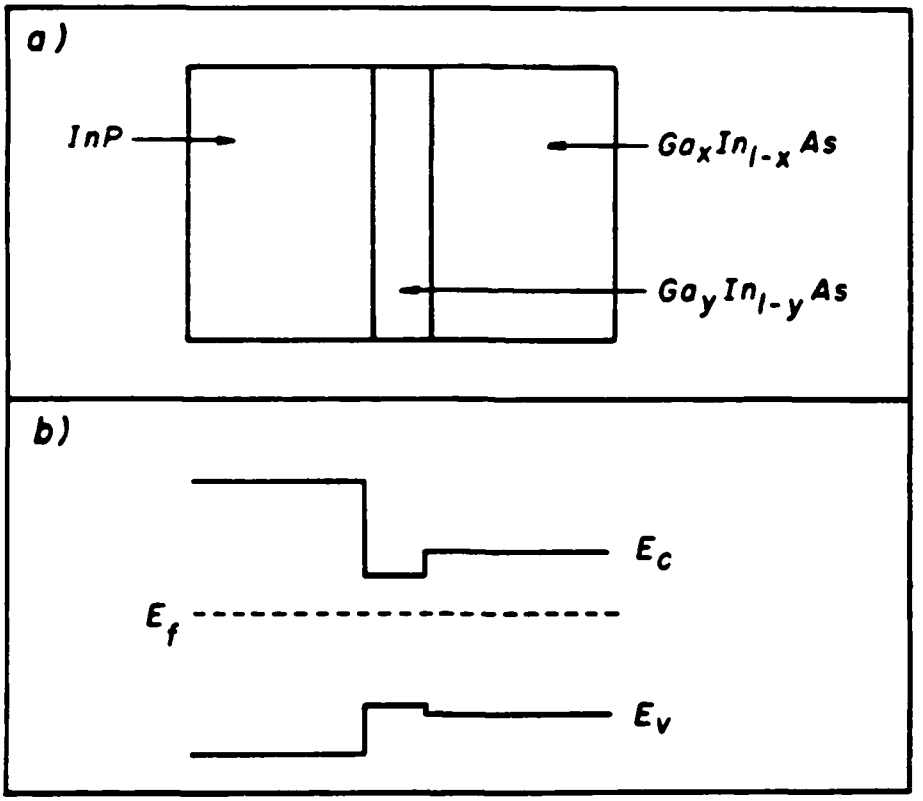

Fig. 1.

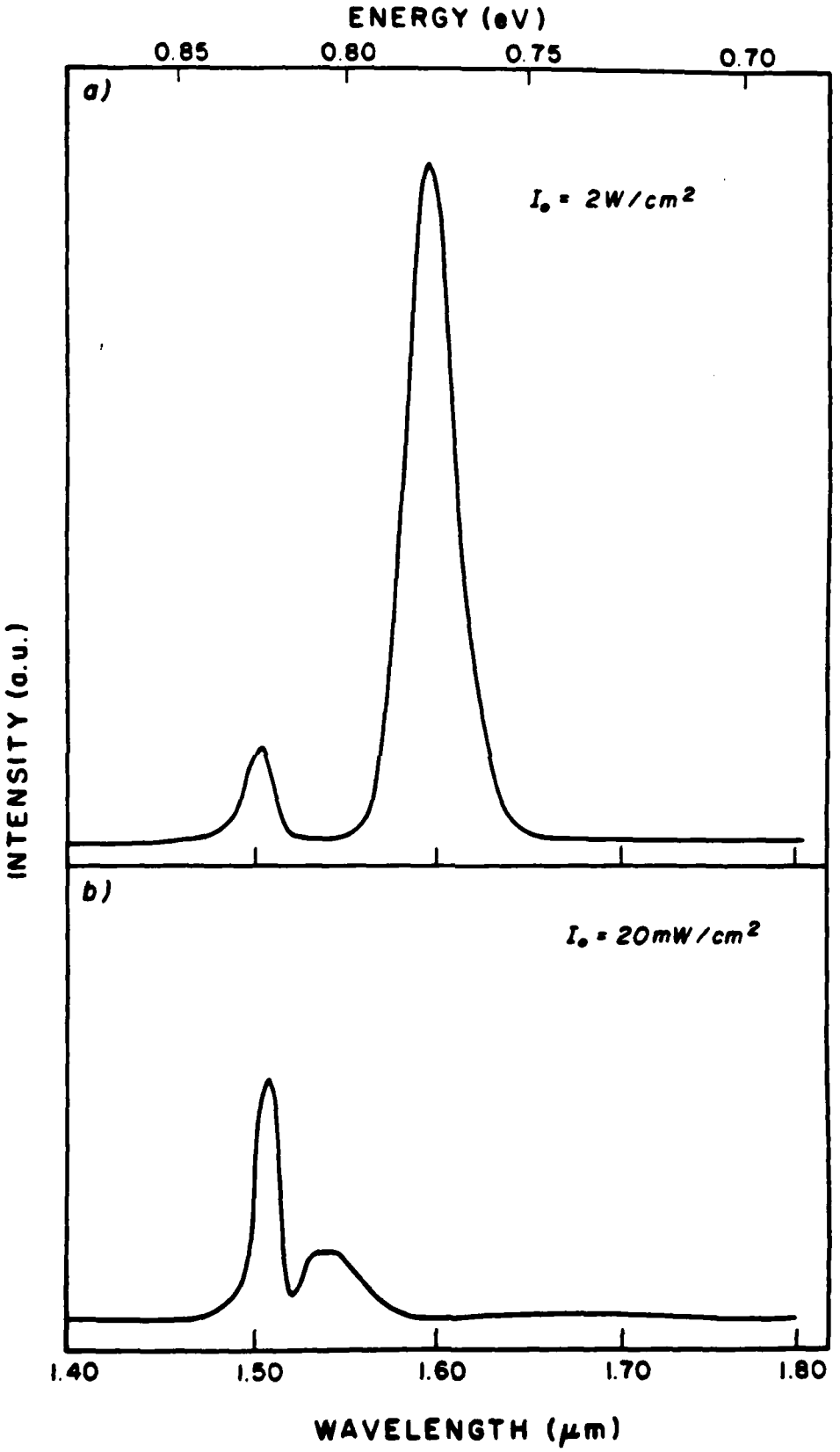
ENERGY (eV)
0.85
0.80
0.75
0.70
a)
I_o = 2W/cm²
b)
I_o = 20mW/cm²
INTENSITY (a.u.)
1.40
1.50
1.60
1.70
1.80
WAVELENGTH (μm)

Fig. 2

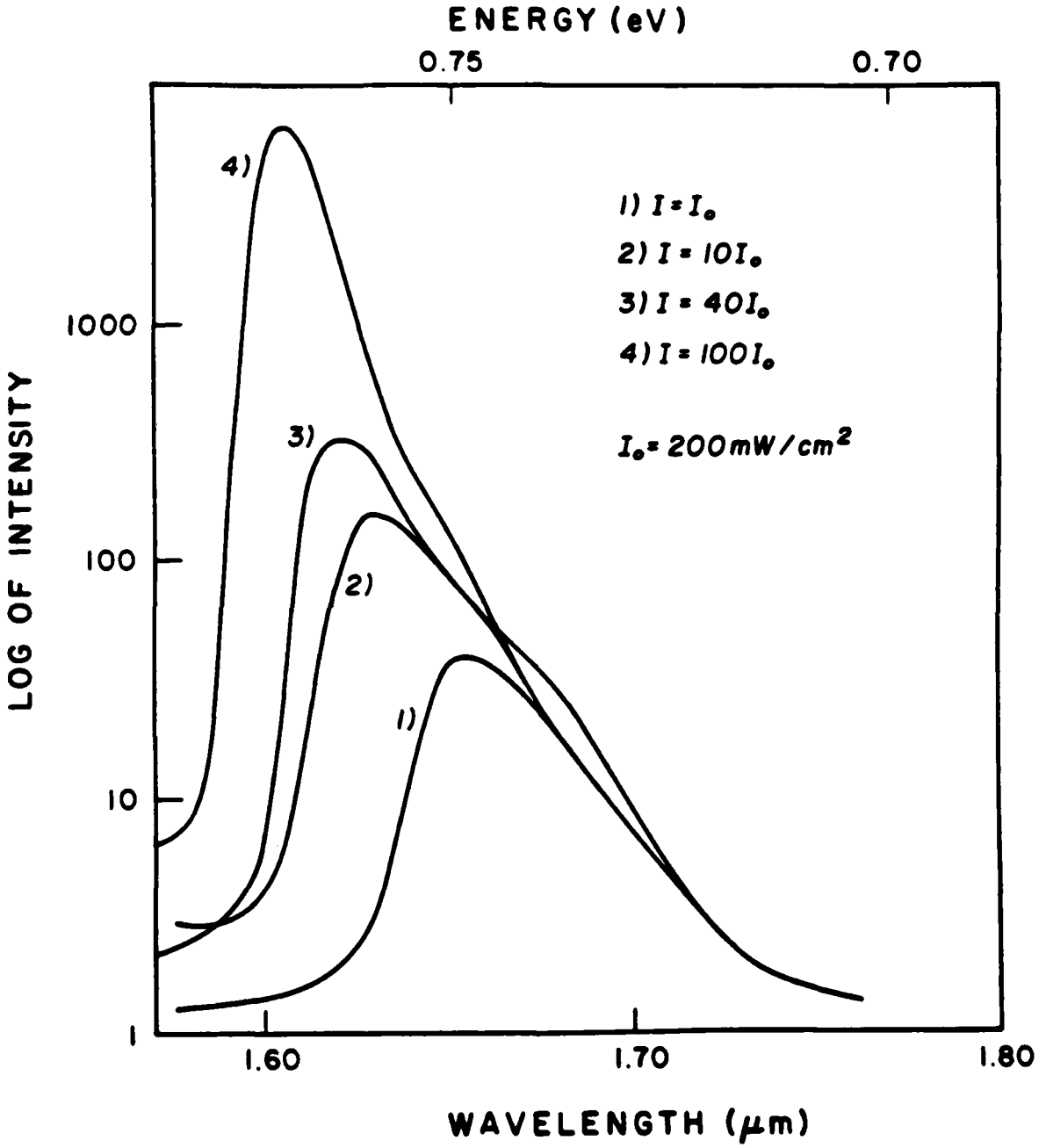
ENERGY (eV)
0.75
0.70
4)
3)
2)
1)
1) I = I₀
2) I = 10I₀
3) I = 40I₀
4) I = 100I₀
I₀ = 200mW/cm²
LOG OF INTENSITY
1000
100
10
1
1.60
1.70
1.80
WAVELENGTH (μm)

Fig. 3.

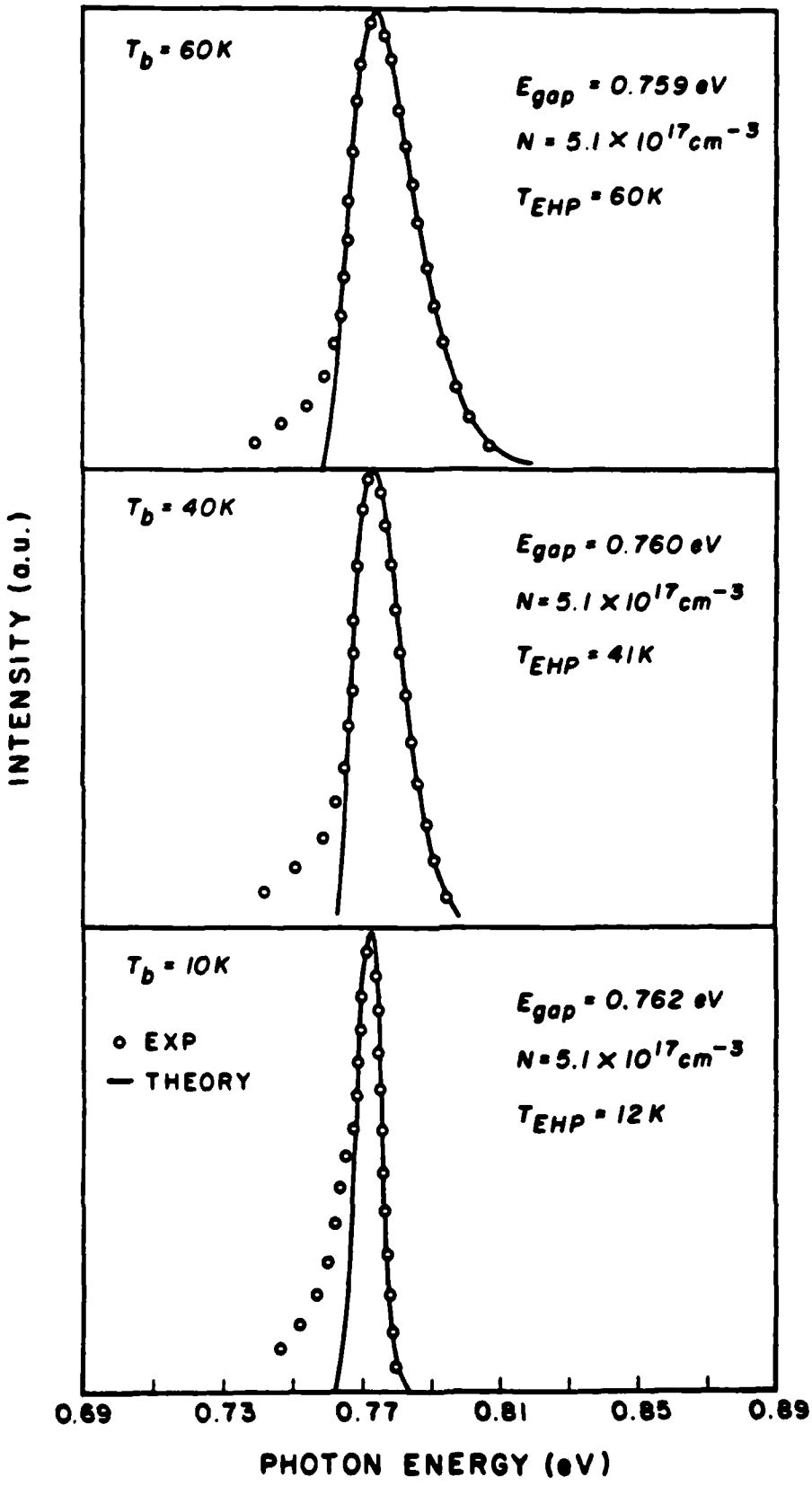
T_b = 60K
E_{gap} = 0.759 eV
N = 5.1 × 10^{17} cm^{-3}
T_{EHP} = 60K
T_b = 40K
E_{gap} = 0.760 eV
N = 5.1 × 10^{17} cm^{-3}
T_{EHP} = 41K
T_b = 10K
o EXP
— THEORY
E_{gap} = 0.762 eV
N = 5.1 × 10^{17} cm^{-3}
T_{EHP} = 12K
INTENSITY (a.u.)
0.69
0.73
0.77
0.81
0.85
0.89
PHOTON ENERGY (eV)

Fig. 4

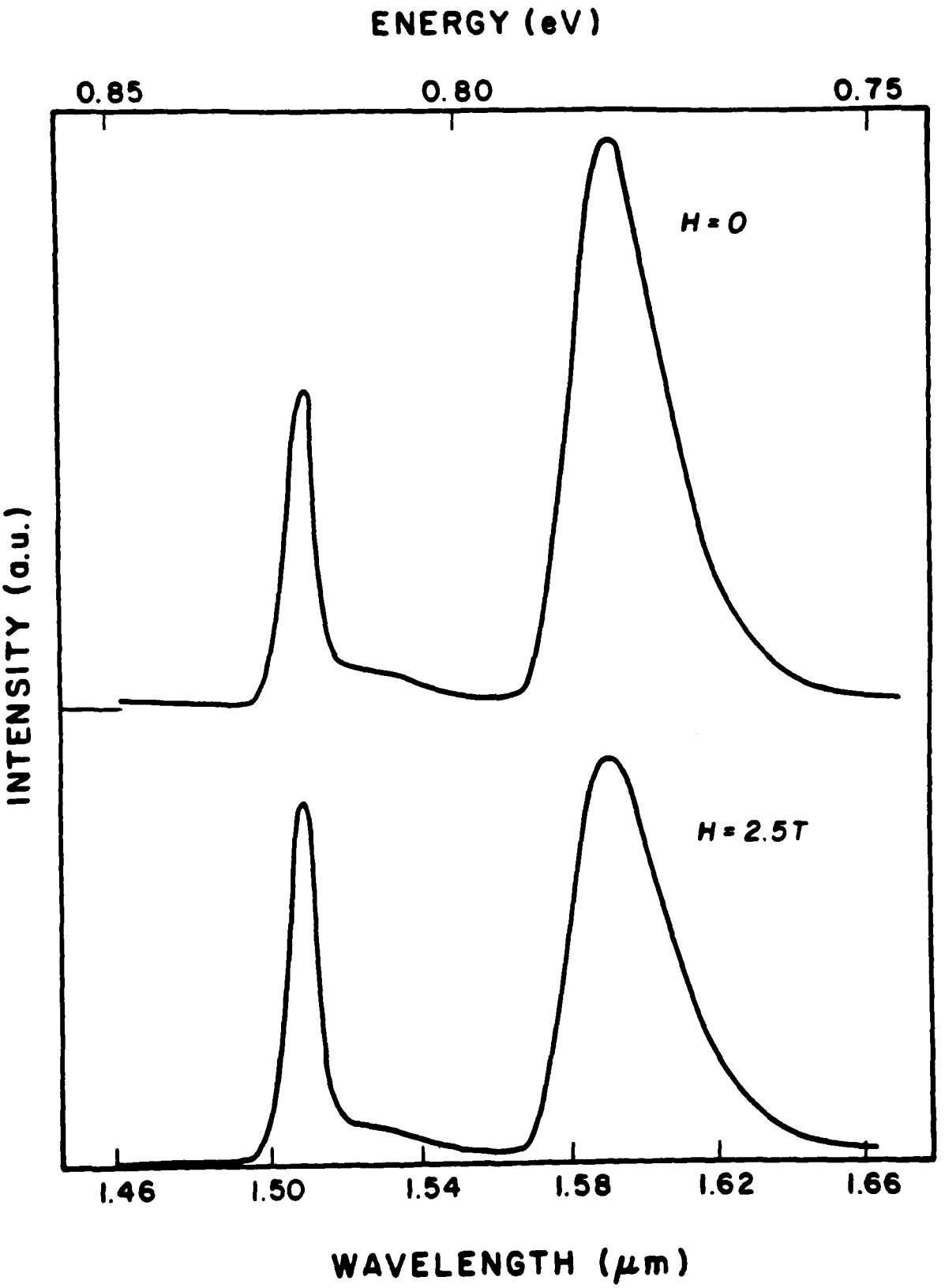
ENERGY (eV)
0.85
0.80
0.75
H = 0
H = 2.5T
INTENSITY (a.u.)
1.46
1.50
1.54
1.58
1.62
1.66
WAVELENGTH (μm)

Fig. 5

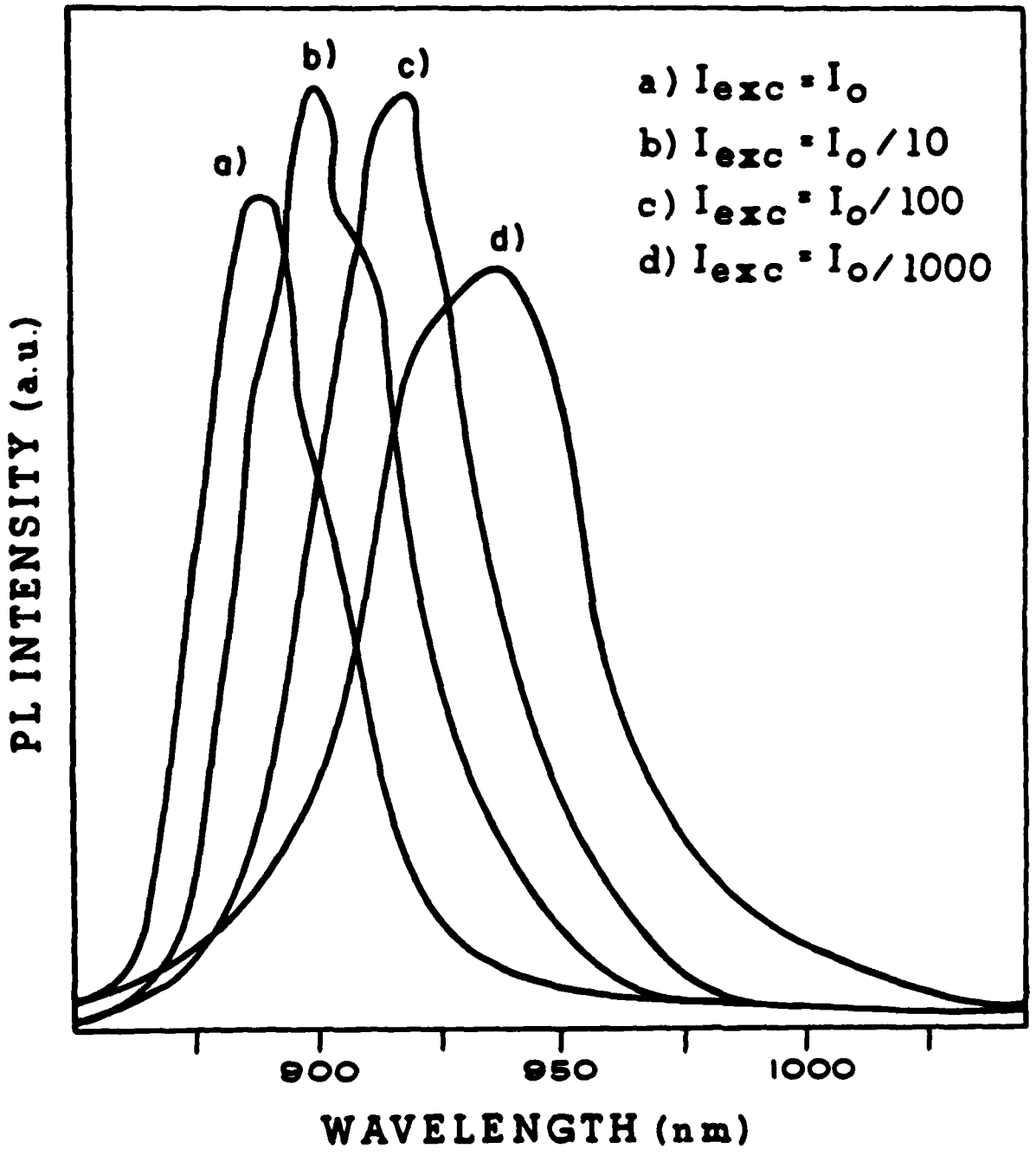
a) $I_{exc} = I_o$
b) $I_{exc} = I_o/10$
c) $I_{exc} = I_o/100$
d) $I_{exc} = I_o/1000$
a)
b)
c)
d)
PL INTENSITY (a.u.)
900
950
1000
WAVELENGTH (nm)

Fig. 5

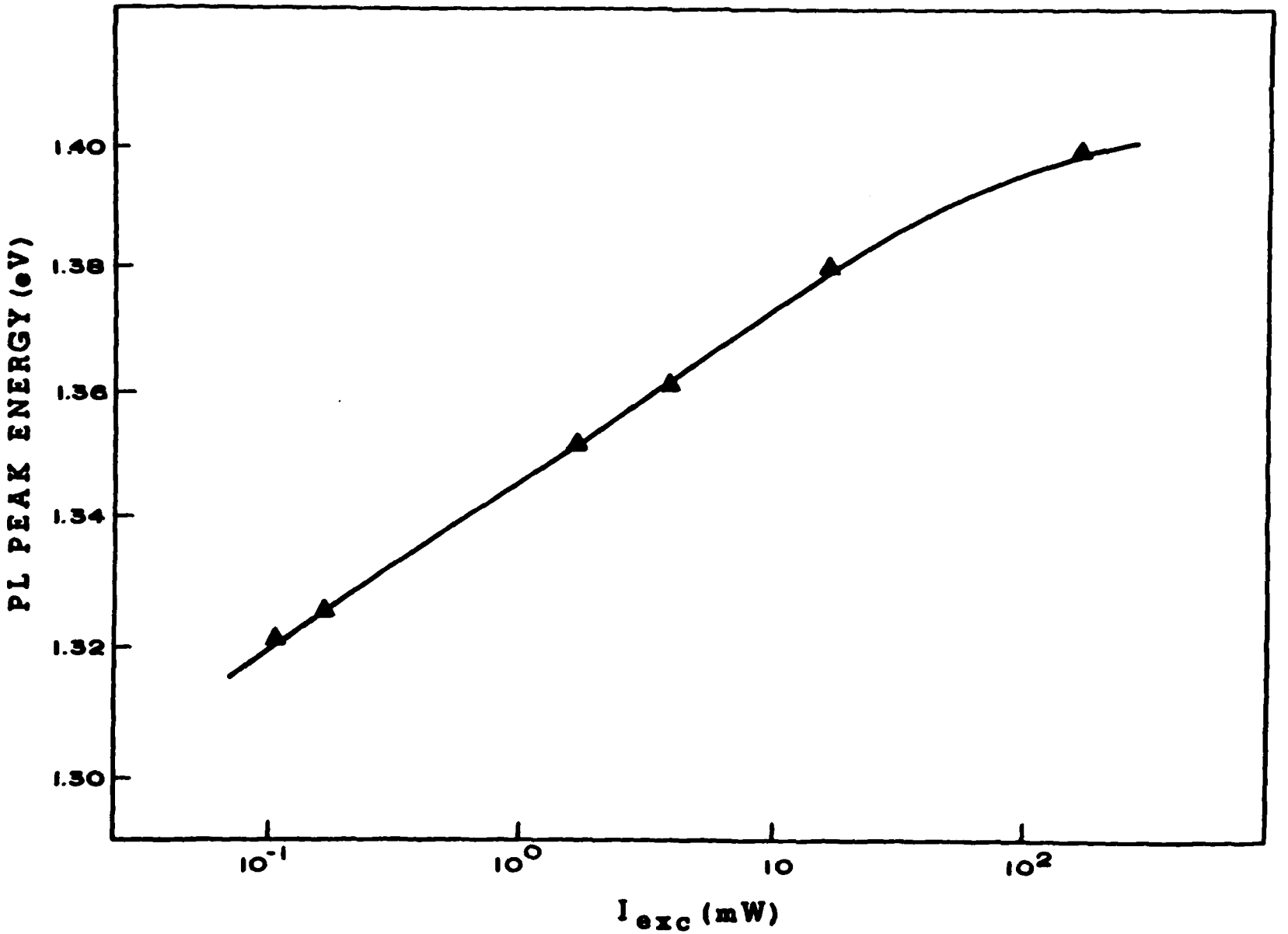

Fig. 7

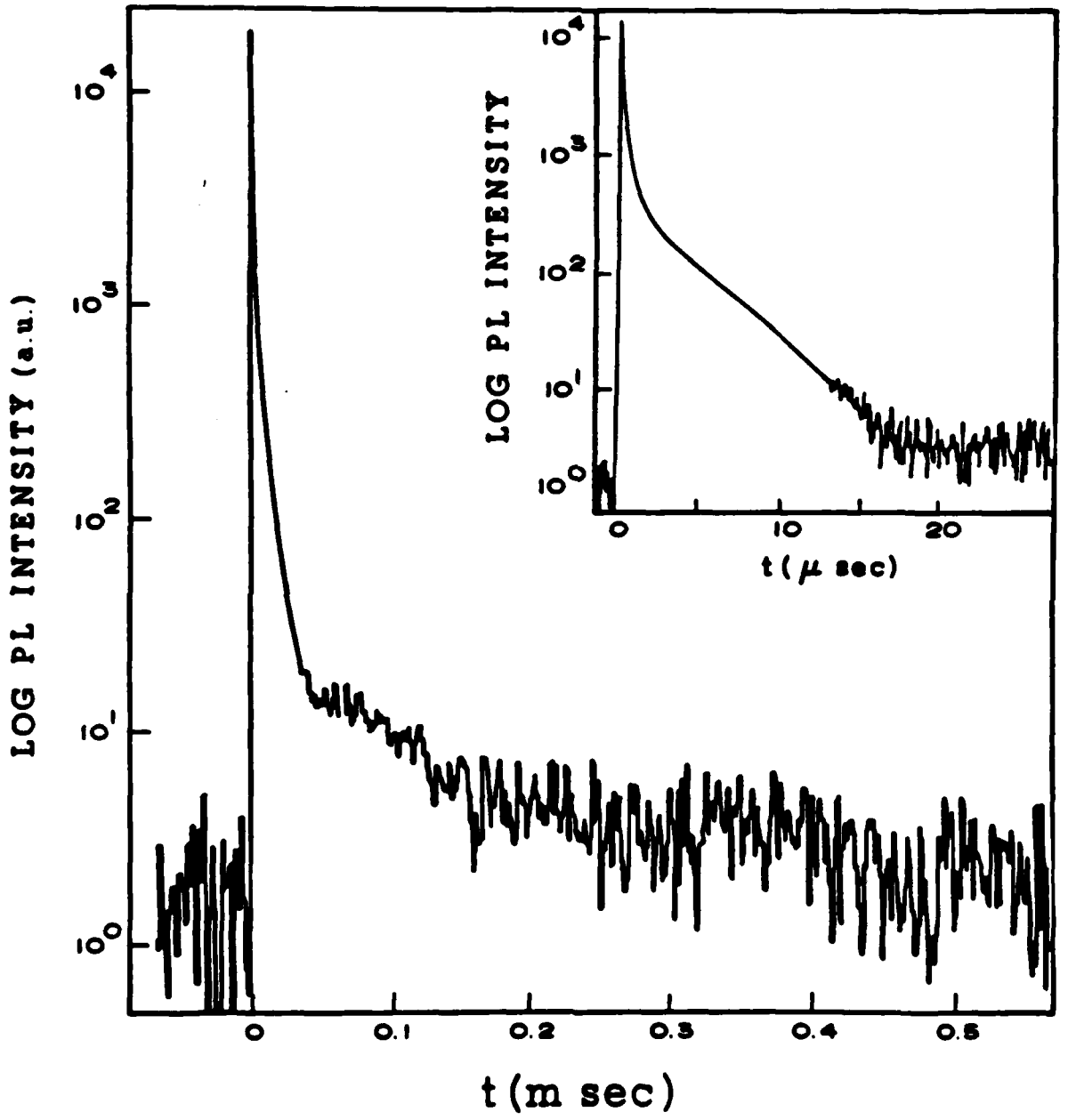
LOG PL INTENSITY (a.u.)
10^4
10^3
10^2
10^1
10^0
0
0.1
0.2
0.3
0.4
0.5
t (m sec)
LOG PL INTENSITY
10^4
10^3
10^2
10^1
10^0
0
10
20
t (μ sec)

Fig. 8

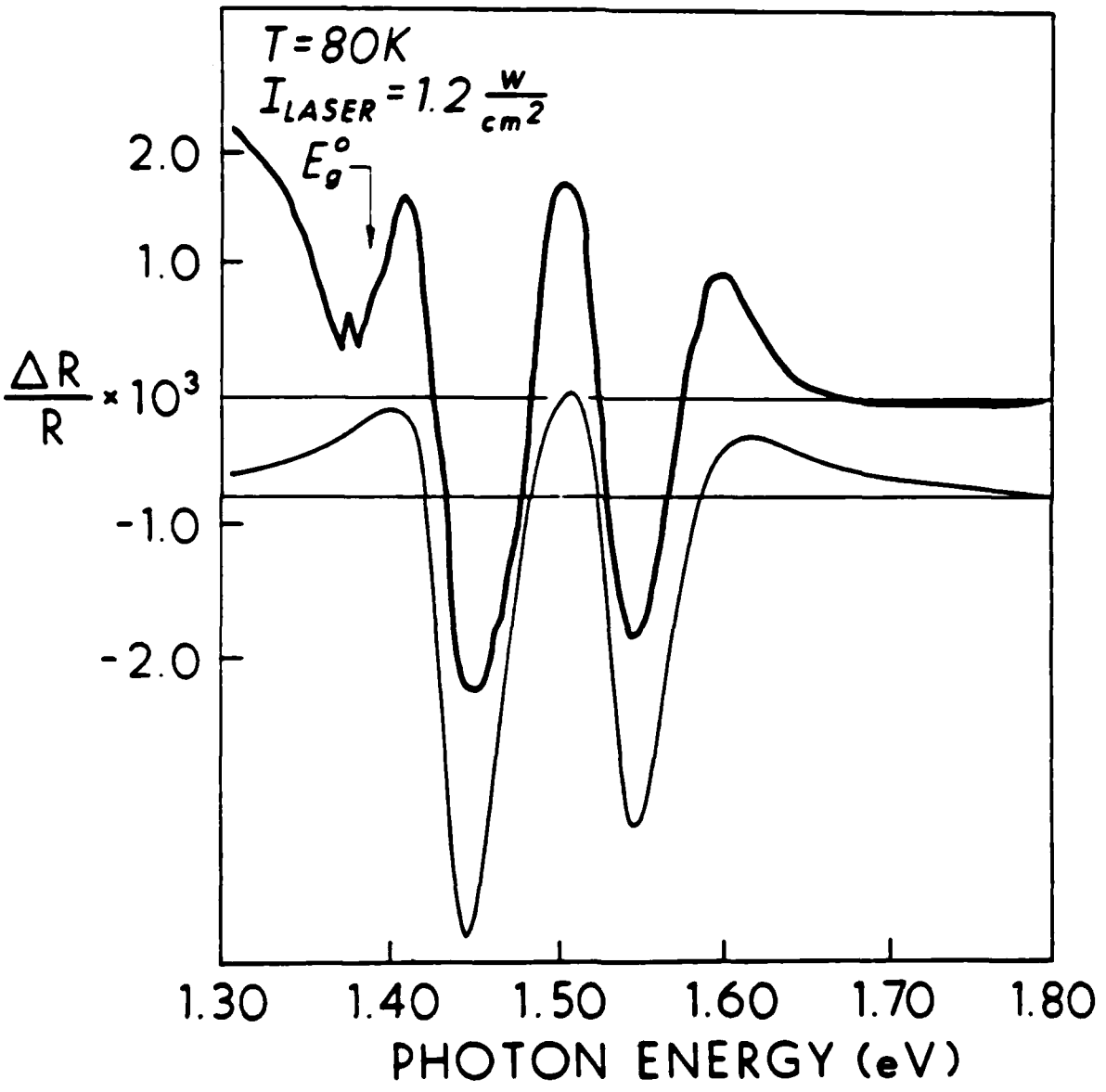
T=80K
$I_{LASER} = 1.2 \frac{W}{cm^2}$
E_g^o
2.0
1.0
$\frac{\Delta R}{R} \times 10^3$
-1.0
-2.0
1.30
1.40
1.50
1.60
1.70
1.80
PHOTON ENERGY (eV)

Fig. 9

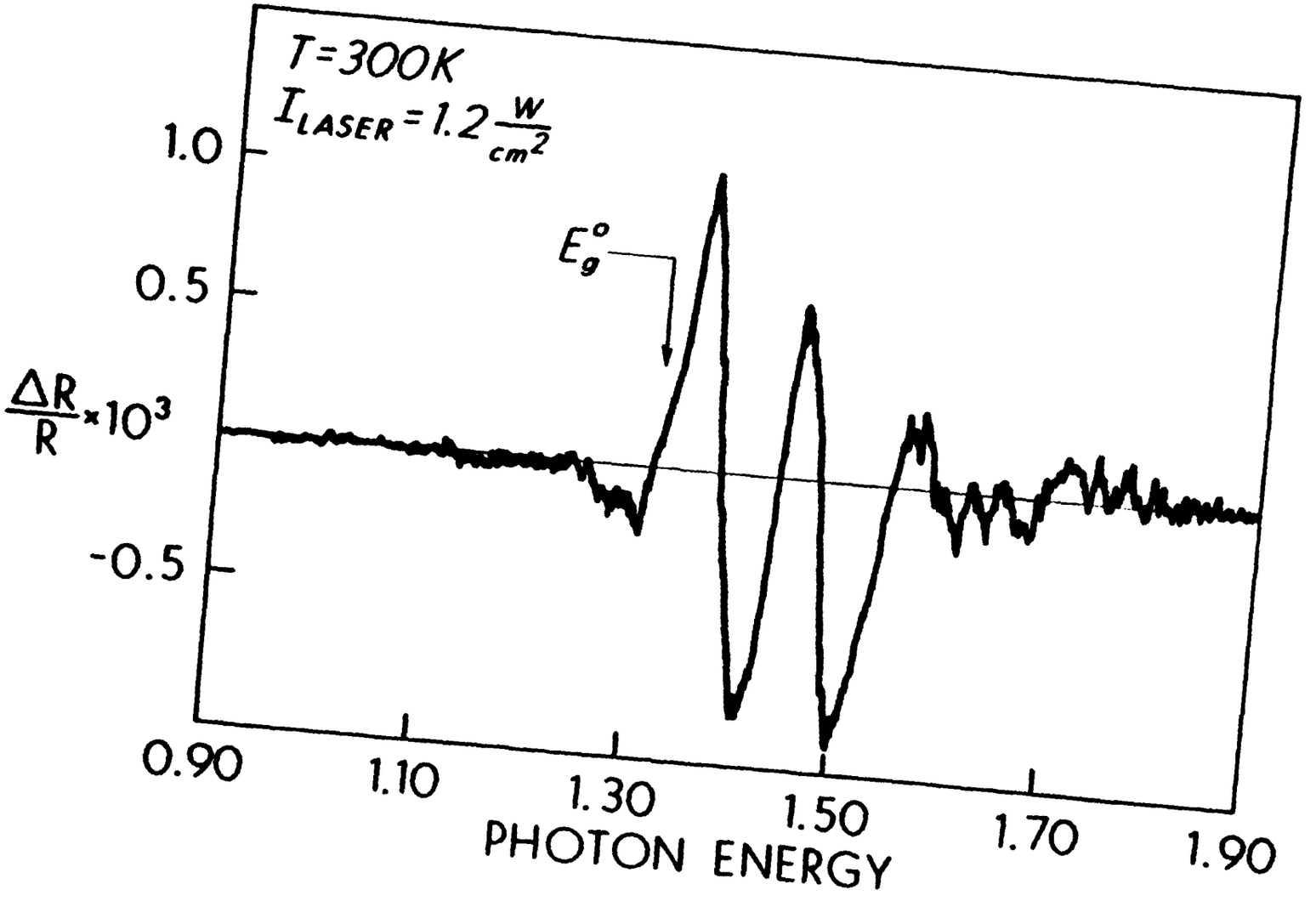
T=300K
$I_{LASER} = 1.2 \frac{W}{cm^2}$
E_g^o
1.0
0.5
-0.5
$\frac{\Delta R}{R} \times 10^3$
0.90
1.10
1.30
1.50
1.70
1.90
PHOTON ENERGY

Fig. 10

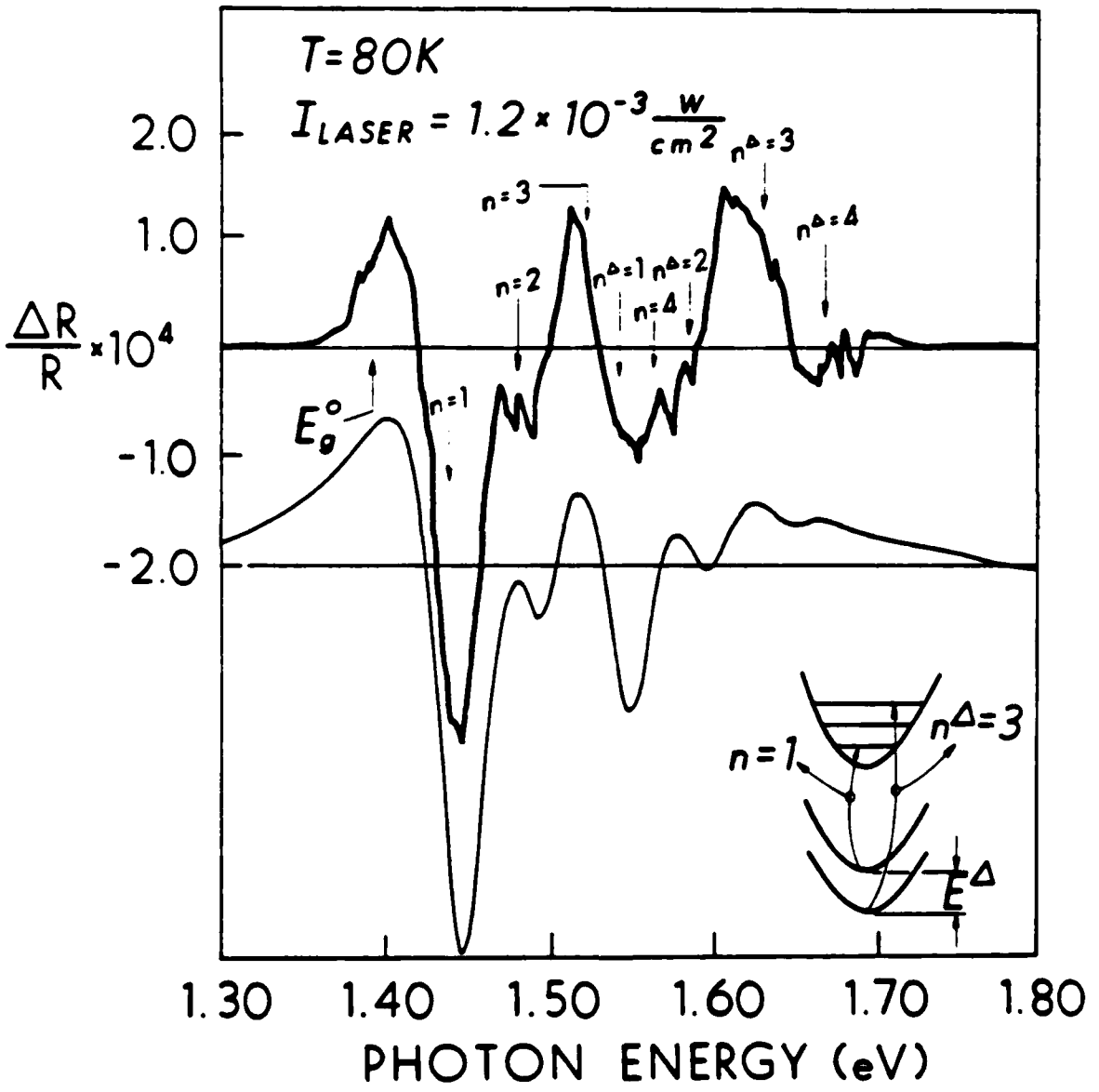
T=80K
$I_{LASER} = 1.2 \times 10^{-3} \frac{W}{cm^2}$
2.0
1.0
-1.0
-2.0
$\frac{\Delta R}{R} \times 10^4$
n=3
$n^\Delta=3$
$n^\Delta=4$
n=2
$n^\Delta=1$
$n^\Delta=2$
n=4
E_0^o
n=1
$n^\Delta=3$
n=1
E^Δ
1.30
1.40
1.50
1.60
1.70
1.80
PHOTON ENERGY (eV)

Fig. 11

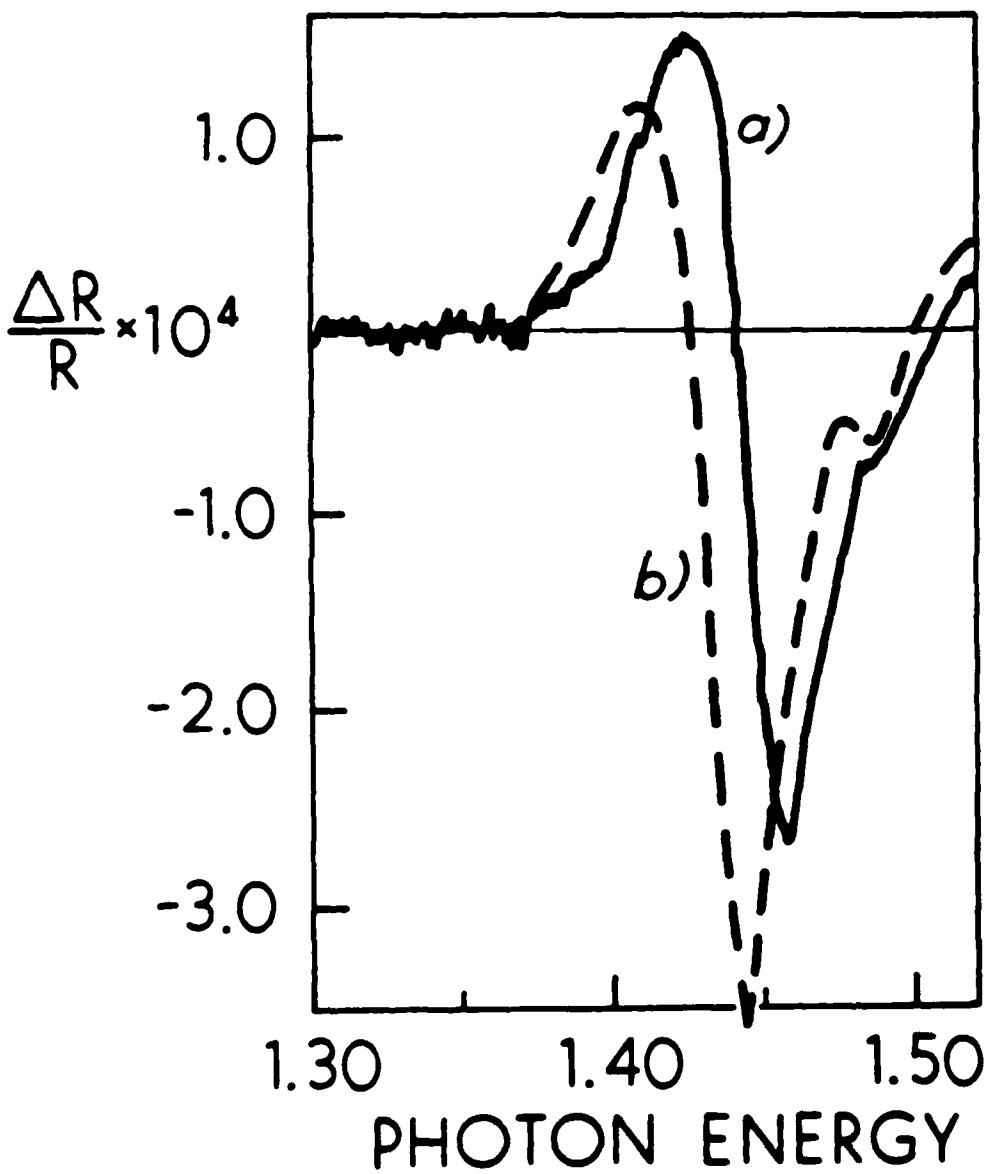
1.0
$\frac{\Delta R}{R} \times 10^4$
-1.0
-2.0
-3.0
a)
b)
1.30
1.40
1.50
PHOTON ENERGY

Fig. 12

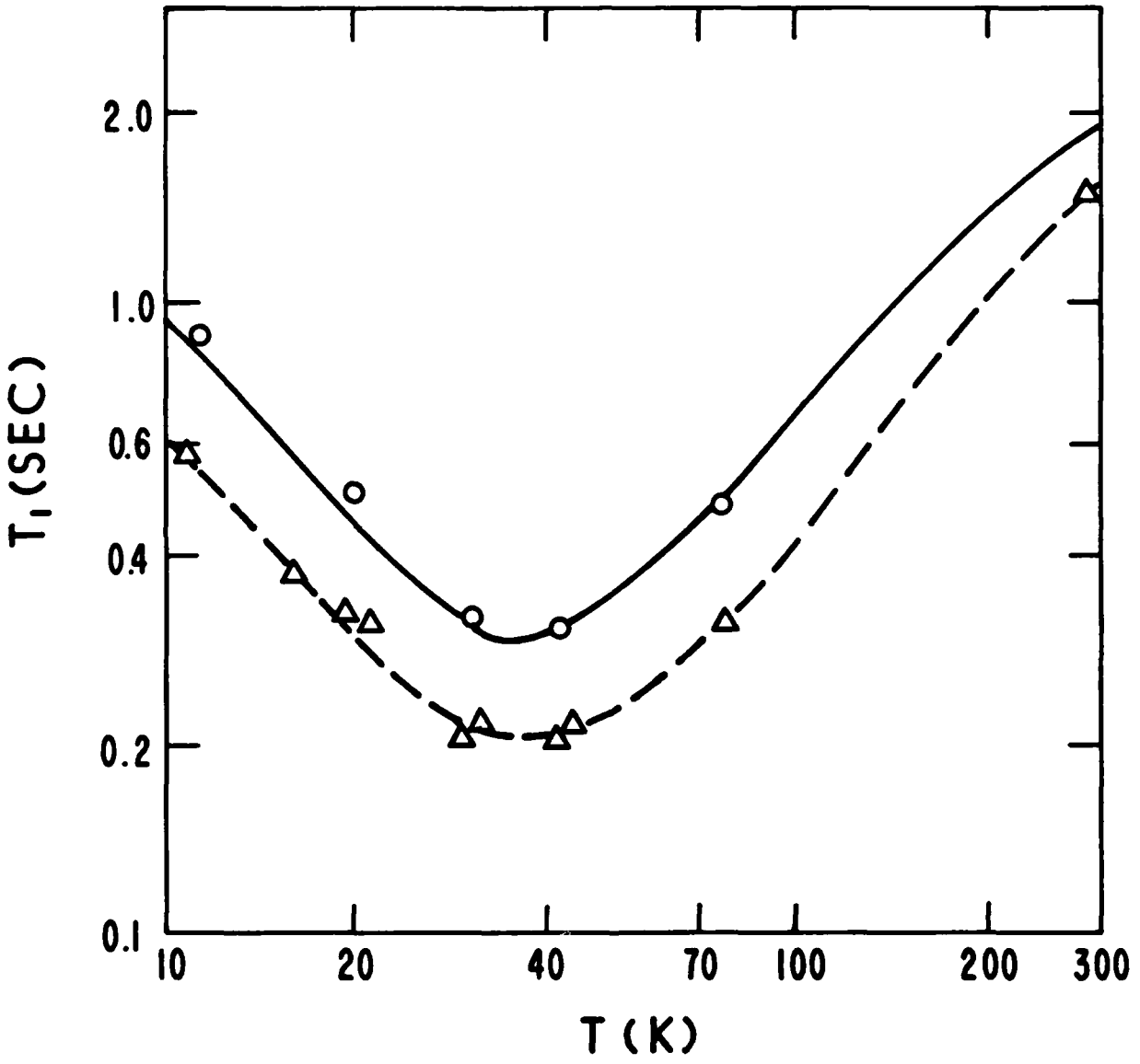

Fig. 13

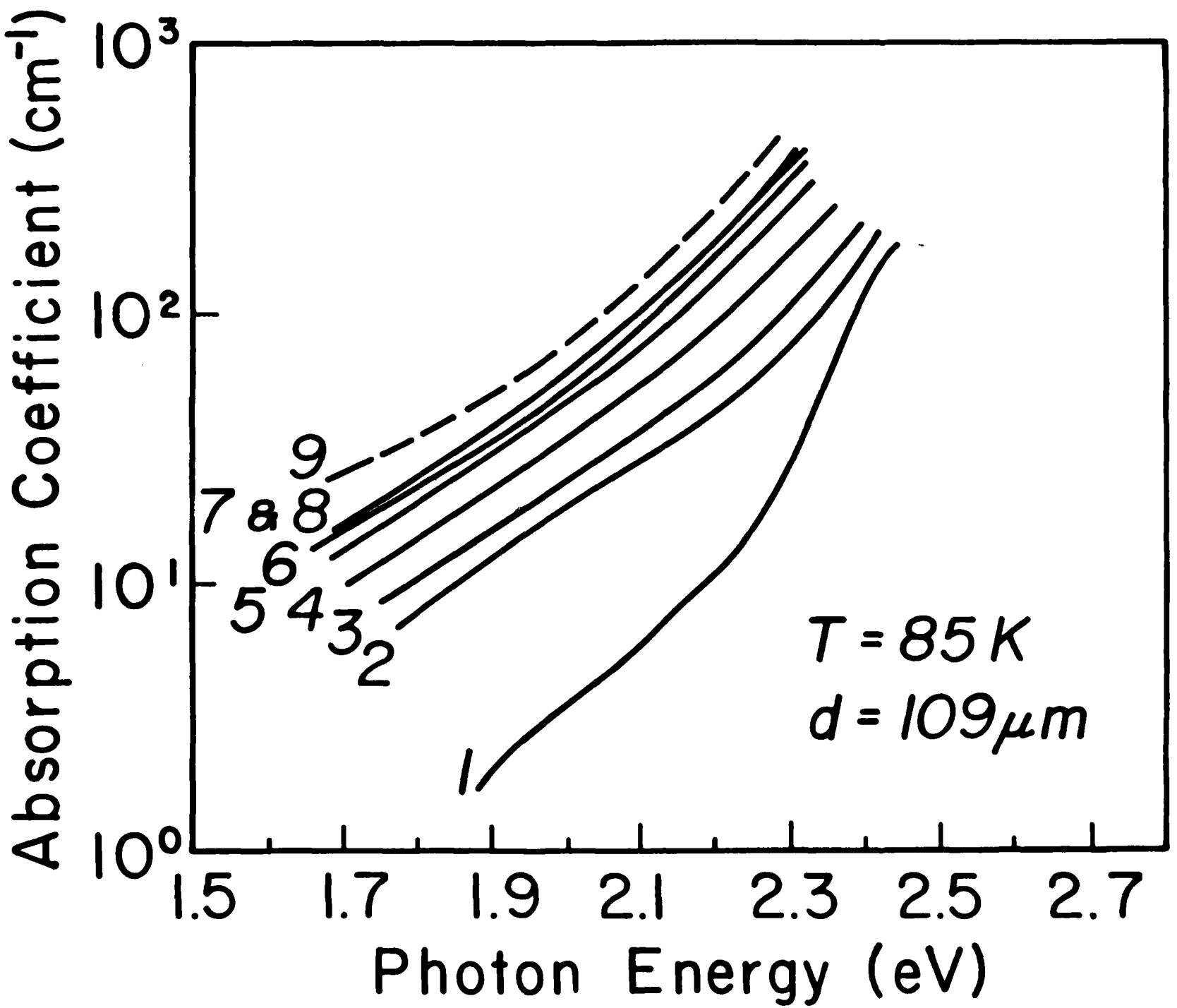
Absorption Coefficient (cm⁻¹)
10³
10²
10¹
10⁰
1.5
1.7
1.9
2.1
2.3
2.5
2.7
Photon Energy (eV)
9
7 & 8
6
5
4
3
2
1
T = 85 K
d = 109 μm

Fig. 14

END

FILMED

6-86

DTIC